Properties of Concentrated Aqueous Electrolyte Solution in a Vicinal Region of Coexisting Solid Surface

Kunikata, Nobuaki
Matsui, Misaki
Maki, Hideshi
Mizuhata, Minoru

(Citation)
ECS Transactions,80(10):1459-1470

(Issue Date)
2017

(Resource Type)
journal article

(Version)
Version of Record

ECS Transactions, 80 (10) 1459-1470 (2017)
10.1149/08010.1459ecst ©The Electrochemical Society

Properties of Concentrated Aqueous Electrolyte Solution in a Vicinal Region of Coexisting Solid Surface

Nobuaki Kunikata[1], Masaki Matsui[1], Hideshi Maki[1, 2] and Minoru Mizuhata[1]

[1] Department of Chemical Science and Engineering,
Graduate School of Engineering, Kobe University,
1-1 Rokkodai-cho, Nada, Kobe 657-8501, Japan
[2] Center for Environmental Management, Kobe University,
1-1 Rokkodai-cho, Nada, Kobe 657-8501, Japan

Properties of concentrated $ZnSO_4$ aqueous solutions coexisting with metal oxide nanoparticles were observed. Raman spectroscopy indicated that ion pair forming tendencies was enhanced in the vicinity of silica nanoparticles which have hydrophilic groups. Zn^{2+} is supposed not to make sufficient hydration sphere and tend to make contact ion pair due to sharing water molecules with hydrophilic solid surface. Alumina nanoparticles exhibited strong effect on ^1H relaxation than silica nanoparticles. The salt concentration dependences of ^1H relaxation time and pH of aqueous solution suggested that the effects from solid phase on coexisting liquid phase were affected by liquid property in itself.

Introduction

Numerous electrochemical devices are expected to operate in higher output using large amount of active materials and concentrated electrolyte solution in limited volume. Large solid/liquid interfacial area between solid phase and liquid phase exist in these systems, and it is well-known that the solid surface affects the properties of water nearby the solid/liquid interface (1). Therefore, solution chemistry not only in bulk solution but also in vicinal area of solid surface is important. In spite of a lot of researchers have been investigating for electrolyte solution, the properties of electrolyte solution\coexisting with solid materials are not studied very well. We have been studying the properties of the coexisting systems consisting of aqueous electrolyte solution and inorganic powder, and confirmed that various kinds of solutions change their properties depending on a distance from solid surface (2 - 4).

Recently, highly concentrated aqueous solution have attracted attention as stable aqueous electrolyte for aqueous lithium secondary batteries (5 - 7). Such electrolyte solutions are regarded as hydrate melts defined by Braunstein which behaves like molten salt in some respects (8). Ionic interaction of ionic species is dominant in liquid properties of such concentrated solutions. In this study, we investigated zinc aqueous solution, because strong ionic interaction of Zn^{2+} makes large hydration sphere, we assumed that interaction from solid surface might be much observable. In order to discuss the interaction in the vicinity of solid phase, we measured the properties of $ZnSO_4$ aq. coexisting with metal oxide nanoparticles focusing on the numerical ratio of water molecules to one salt and interfacial liquid molecular layer thickness.

Experimental

Sample preparation

$ZnSO_4$ aqueous solution was prepared by dissolving zinc sulfonate heptahydrate in deionized distilled water. Concentration of aqueous solutions were determined using inductively coupled plasma atomic emission spectroscopy (HORIBA). The concentration dependence of pH for $ZnSO_4$ aqueous solution was displayed as Fig. 1. Fumed metal oxides supplied from Nippon Aerosil were used as solid phase, and solid/liquid coexisting samples were obtained mixing the fumed oxides with $ZnSO_4$ aq. thoroughly using an agate mortar. Volume fractions of the liquid phase ranged from 85.0 to 100 vol%. The physical aspects of the oxides are shown in Table 1 (9). The crystalline phases of fumed metal oxides were assigned using parallel beam X-ray diffractometer RINT-TTR (Rigaku), following the references as shown in the Table. The relative weight fraction of rutile was 7.7 wt% as Moiseev et al. reported by Rietveld refinement.

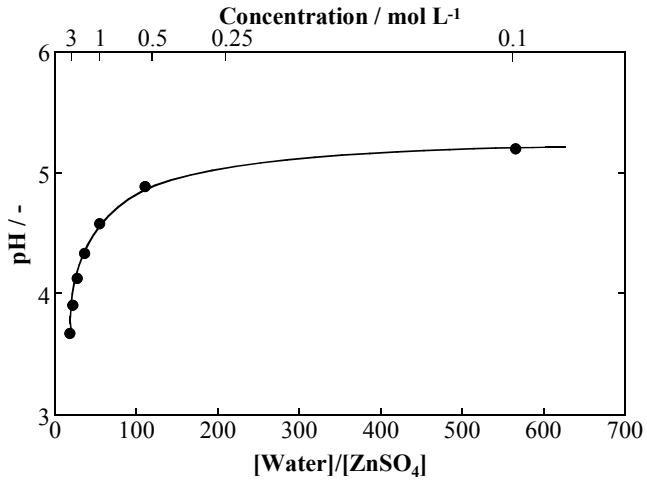

Figure 1. Concentration and numerical ratio dependences of pH for $ZnSO_4$ aq. at 25 ºC.

TABLE I. Properties of the fumed metal oxides.

Samples	Nature	Specific surface area / $m^2\ g^{-1}$	Average particle size / µm	Origin
Fumed silica	SiO_2 (Amourphous)	200±25	12	Aerosil 200
Fumed alumina	γ - Al_2O_3 [10]	130±15	10	Aeroxide Alu 130
Fumed titania	TiO_2 (Rutile, Anatase) [11]	90±20	14	Aeroxide TiO_2 P90

Thermal analysis

Phase transition behavior was observed by DSC with a Thermo Plus DSC 8230L (Rigaku) with liquid nitrogen cooling unit. The fumed metal oxides were thoroughly mixed with $ZnSO_4$ aqueous solution, then the solid/liquid coexisting samples were immediately sealed in an aluminum sample pan. The employed scanning temperature range was between -70 and 50°C and the scan rate was 5°C per minute. Cooling and heating processes were repeated more than three times in dry nitrogen atmosphere.

Temperature and heat flow calibration were carried out using the melting points of 1,2-dichloroethlene (mp = -35.3°C) and In (mp = 156.6°C). The obtained DSC curves were corrected to determine the melting point and heat of fusion for the liquid phase by subtracting baseline.

Density measurement

Densities of liquid sample were measured using DMA 5000M with oscillating U-tube sensor (Anton Paar). We obtained vibrational frequencies and converted to densities.

Raman spectroscopy

Raman spectra were recorded by T-64000 Raman spectrometer equipped with a YAG laser with a charge coupled device detector cooled using liquid nitrogen. The 532 nm line of Nd: YAG laser was used for excitation. The solid/liquid coexisting samples were loaded into glass tubes and set in the 180° scattering geometry. The wavenumber of monochrometer was calibrated by silicon at 520 cm^{-1}. All experiments were performed at 25 ± 0.5°C.

^{1}H Relaxation measurement

The spin-lattice relaxation time (T_1) and spin-spin relaxation time (T_2) in ^{1}H NMR were obtained by relaxation time measuring equipment Acorn area (XiGo Nanotools). The solid/liquid coexisting samples were put into 5 mm diameter glass NMR tube. All experiments were performed at 25 ± 0.5°C.

Zeta potential measurement

For studying surface potential of metal oxide nanoparticles, ELS-Z2 (Otsuka Electronics) based on laser Doppler method equipped with pH titrating system was used. 0.1 mol L^{-1} NaCl aq. and 1 wt% of the metal oxide nanoparticles were utilized to prepare the suspensions, which then were treated in an ultrasonic bath for 20 min. The low oxide content was used in order to avoid hydrodynamic and electrostatic interactions between particles. The pH values were adjusted by 0.1 mol L^{-1} HCl or NaOH aqueous solutions containing 0.1 mol L^{-1} NaCl. We confirmed surface potential of SiO_2 and Al_2O_3 depending on pH as shown in Fig. 2.

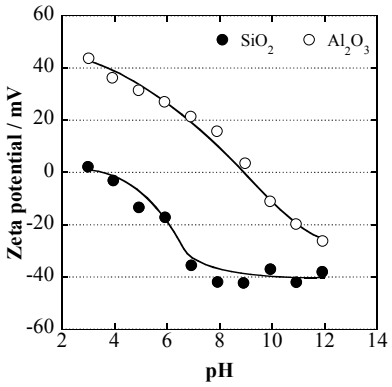

Figure 2. Relationships between surface potential of 0.1 wt% of SiO_2 and Al_2O_3 nanoparticles and pH of dispersion medium: 0.1 mol L^{-1} NaCl aq.

Results and Discussion

Phase Diagram and Electrostriction of Bulk Aqueous Solution

Water and zinc sulfate heptahydrate system showed binary phase diagram as shown in Fig. 3. The eutectic composition was 0.050 mole fraction of zinc sulfate. DSC measurement revealed two endothermic peaks in heating process of $ZnSO_4$ aq. The Peaks appeared at lower temperature were assigned to the liquidus line in the phase diagram, and the higher ones were linked with the solidus line. Kanagadurai et al. reported that crystals of heptahydrate grew by temperature lowering $ZnSO_4$ solution technique (12). In addition, we didn't observe thermal transition under the solidus line temperature. The eutectic composition suggested that 19 water molecules and one salt exhibit phase transition. Rudolph et al. reported that Zn^{2+} have 6 water molecules as first hydration sphere and 12 water molecules as second hydration sphere (13). Considering first and second hydration number, phase transition at the eutectic composition was supposed to take along almost all water molecules in liquid system. This numerical ratio of water molecules per one salt is high compared with other H_2O-salt system (14 - 18).

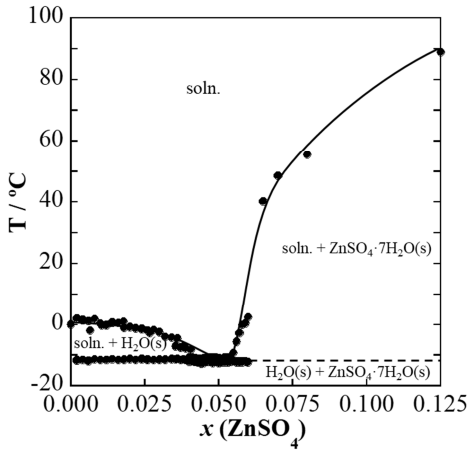

Figure 3. Phase diagram of H_2O-$ZnSO_4$ system.

The volume subtraction was calculated by following equation using the concentration dependence of liquid density shown in Fig. 4, and plotted with numerical ratio of water molecules per one salt which was converted from concentration.

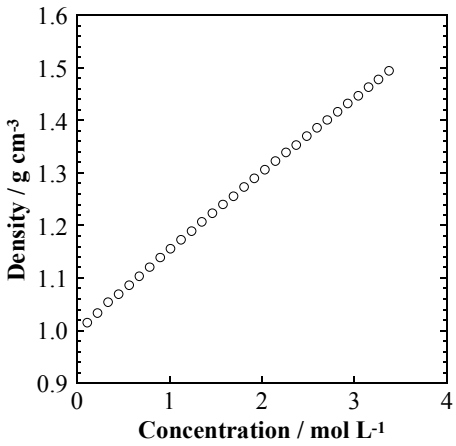

Figure 4. Concentration dependence of density for $ZnSO_4$ aq. at 25 ºC.

$$\text{Volume change by 1 mol of water} = \frac{\Delta(\text{solution volume per mol of salt})}{\Delta(\text{mol of water per mol of salt})}$$

$$= \frac{\Delta(1/\text{Concentration})}{\Delta([\text{Water}]/[\text{Salt}])} = \frac{\left|\frac{1}{\text{Concentration}}\right|_{n+1} - \left|\frac{1}{\text{Concentration}}\right|_{n}}{\left|\frac{[\text{Water}]}{[\text{Salt}]}\right|_{n+1} - \left|\frac{[\text{Water}]}{[\text{Salt}]}\right|_{n}} \quad [1]$$

Fig. 5 represents volume increment by adding one mole of water to one mole of salt. The volume increment was 18ml mol^{-1} in dilute solution and decreased under about 40 water molecules per one salt in Fig. 5(a). This decrease is known as electrostriction caused by ionic species and remarkable compared with other salt like lithium nitrate shown in Fig. 5(b) (19). The phase diagram and the results of volume subtraction shows that zinc sulfate affects many water molecules than other salts due to its strong ionic interaction.

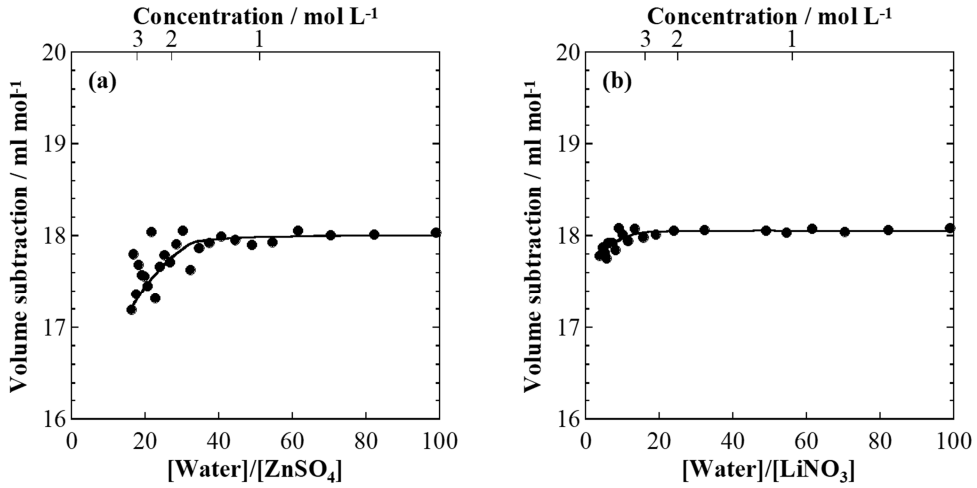

Figure 5. Concentration and numerical ratio dependences of volume change for (a) H_2O-$ZnSO_4$ system and (b) H_2O-$LiNO_3$ system.

Thermal analyses for Metal Oxide Nanoparticles/Water system

Thermal analyses were carried out for metal oxide nanoparticles/water system to investigate the influence from solid surface on water molecules. The DSC curves during heating process for various specimens are shown in Fig. 6. For each metal oxide sample and liquid volume fraction, the endothermic peak for fusion of ice was observed. These peaks shifted toward the lower temperature with the decrease of the liquid content. This behavior was similar to our previous studies and we reported that the thermochemical property of liquid phase depends on the hydrophilicity of the coexisting solid surface (20).

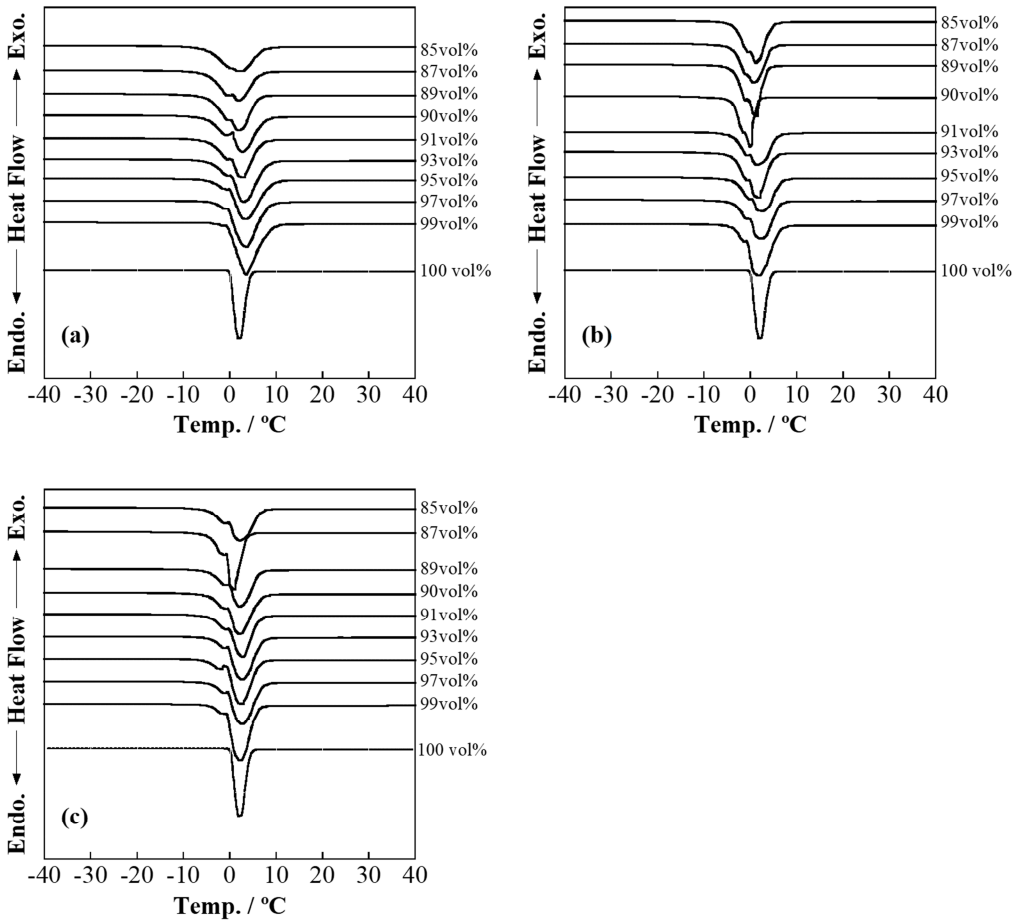

Figure 6. Variations of DSC curves with liquid content for the different metal oxide nanoparticles/water system; (a) SiO_2, (b) Al_2O_3, and (c) TiO_2 nanoparticles. Each curves were normalized per unit weight of liquid phase.

In order to discuss dynamics of solvent molecules in restricted area between dispersed nanoparticles, we proposed the spatial model that liquid layer is on solid surface and such particles are monodispersed as hexagonal close-packed described in Fig. 7. Consequently, we defined the parameter called “apparent average thickness” by the following equations. This parameter replaces volume fraction with the overall liquid layer distance, which has a dimension of length.

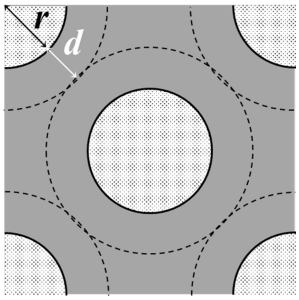

Figure 7. Schematic model of solid/liquid coexisting system; *d* and *r* means apparent average thickness and solid particle radius, respectively.

$$V = 16\sqrt{2}(r+d)^3 \qquad [2]$$

$$d = r\left[\left(\frac{\pi}{3\sqrt{2}}\cdot\frac{1}{1-V_L}\right)^{\frac{1}{3}} - 1\right] \qquad [3]$$

d : Apparent average thickness
r : solid radius
V : unit cell volume
V_L : liquid phase volume

Fig. 8 shows relationships between the apparent average thickness and the heat of fusion of ice coexisting with metal oxide nanoparticles; SiO_2, Al_2O_3, and TiO_2. The heat of fusion showed deviation from the line of the bulk system and decreased as apparent average thickness gets smaller than about 10 or 20 nm. It suggests that the effect of coexisting solid phase reaches dozens of water molecules in the vertical direction with respect to the solid surface. Zobel reported that three to five layers of restructured water molecules exists in water–nanoparticle interfaces using spectroscopic methods like X-ray scattering (21). The length of liquid layer in which the effect from solid surface was observed in heat of fusion was much longer compared with the value Zobel reported. It is assumed that the effect from solid phase based on hydrogen bond networking might range over dozens of solvent molecules from solid surface, and it is hard to express only by electrical double layer or static liquid structure observed by X-ray scattering and so on.

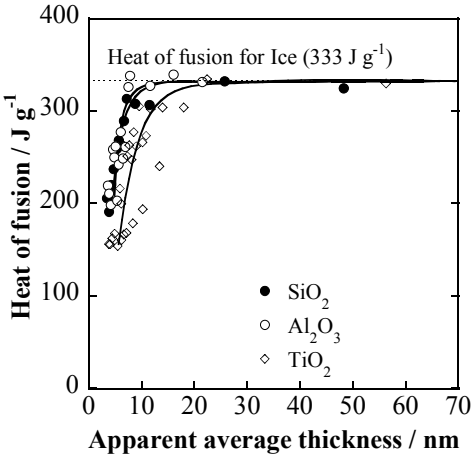

Figure 8. Apparent average thickness dependences of heat of fusion of H_2O coexisting with metal oxide nanoparticles.

Raman spectra for Silica Nanoparticles/$ZnSO_4 \cdot nH_2O$ system

Fig. 9 shows Raman spectra for $ZnSO_4$ aqueous solution. Sulfate anion have four equivalent oxygen atoms and its symmetrical stretching vibration was observed around 982 cm^{-1}. As $ZnSO_4$ concentration increase, the peak intensity increased and wavenumber of the peaks changed to high frequency side. As Rudolph et al. reported, the symmetrical stretching vibration in $ZnSO_4$ aq. exhibit a small shoulder on the high frequency side with concentration increase and the high frequency shoulder is attributed to the formation of a 1:1 inner-sphere contact ion pair by Zn^{2+} and SO_4^{2-} (22 - 24). We confirmed the same behavior not only in bulk solution but also in solid/liquid coexisting system. Fig. 10 is concentration and numerical ratio dependences of wavenumber of peak observed for SiO_2 nanoparticles/$ZnSO_4 \cdot nH_2O$ system. The wavenumber of peak for bulk $ZnSO_4$ aq. remarkably changed when number of water molecules per one salt was under ca. 40, which was similar to the results of density measurement obtained as Fig. 3(a). In solid/liquid coexisting system, the wavenumber of the peak changed to high frequency side in lower concentration compared with bulk $ZnSO_4$ aq., consequently ion pair forming tendencies seems to be enhanced. Since apparent average thickness of coexisting samples shown in Fig. 8 were smaller than 8 nm, these liquid phase seems to be affected by solid surface. Zn^{2+} was not supposed to make hydration sphere sufficiently due to sharing water molecules with solid surface, and ion paring tendencies seems to be enhanced in the vicinity of solid surface. This result agrees with the previous study for the α-Al_2O_3 powder/$ZnCl_2 \cdot nH_2O$ system, which suggested that the structural change of the ionic species affect ionic conduction behavior (18).

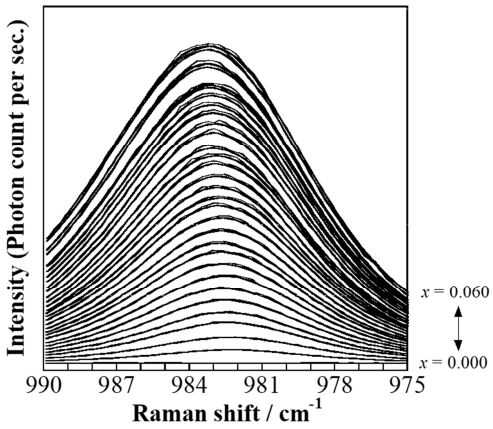

Figure 9. Raman spectra of $ZnSO_4$ aq. at 25 ºC. Each curves were displaced at intervals of 0.002 mole fraction of $ZnSO_4$.

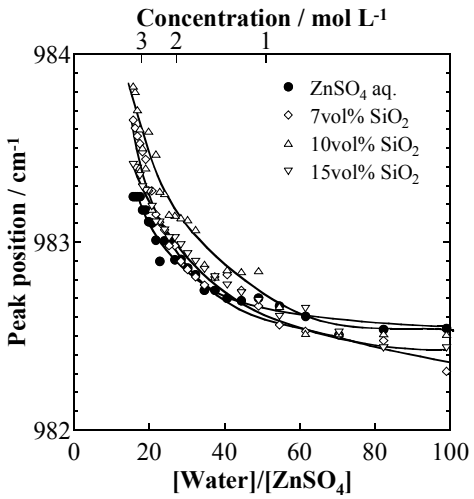

Figure 10. Concentration and numerical ratio dependences of Raman band position for SiO_2 nanoparticles/$ZnSO_4 \cdot nH_2O$ system.

^{1}H relaxation time for Metal Oxide Nanoparticles/$ZnSO_4 \cdot nH_2O$ system

Fig. 11 shows concentration and numerical ratio dependences of T_1 and T_2 for SiO_2 nanoparticles/$ZnSO_4 \cdot nH_2O$ system. T_1 and T_2 of bulk $ZnSO_4$ aq. decreased as the salt concentration increase. It shows mobility of water molecules in aqueous solution was suppressed by ionic interaction. T_1 of $ZnSO_4$ aq. coexisting with SiO_2 nanoparticles was slightly lower than the bulk value as shown in the figure, while volume fraction dependences were subtle. However, T_2 of $ZnSO_4$ aq. coexisting with SiO_2 nanoparticles exhibited drastic decrease depending on solid/liquid volume fraction. The water molecules in the aqueous solution reduce its mobility by not only ionic interaction but also coexisting solid surface.

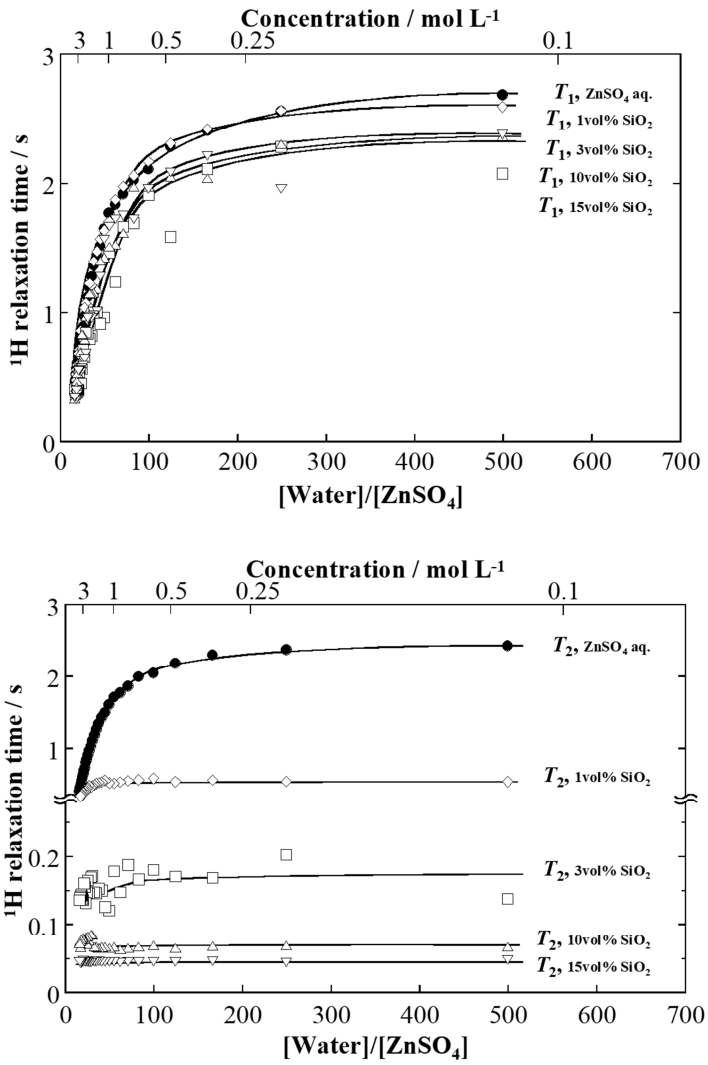

Figure 11. Concentration and numerical ratio dependences of ^{1}H relaxation time (T_1, T_2) for SiO_2 nanoparticles/$ZnSO_4$·$n$$H_2O$ system; (a) T_1 and (b) T_2. The hydration number n represents the numerical ratio; [Water]/[$ZnSO_4$] in the figure.

The concentration and numerical ratio dependences of T_1 and T_2 for the system with SiO_2 and Al_2O_3 nanoparticles were obtained as shown in Fig. 12. Although the T_2 of $ZnSO_4$ coexisting with 15 vol% of SiO_2 decreased from the bulk solution, the T_1 of bulk solution and $ZnSO_4$ aq. coexisting with 15 vol% of SiO_2 nanoparticles approached to the same value as salt concentration increase. On the other hand, coexisting system with Al_2O_3 nanoparticles showed significant decrease in both the T_1 and T_2. Al_2O_3 seems to exhibit strong effect on aqueous solution than SiO_2 and effect from solid surface is relatively large. The differences between the SiO_2 and the Al_2O_3 nanoparticles might be related to surface potential of each metal oxide nanoparticles as shown in Fig. 2. It is well known that zinc aqueous solution indicates acidity due to the hydrolysis by Zn^{2+}. The pH in Fig. 1 decreased with the concentration increase. The solid surface of SiO_2 nanoparticles exhibits negative charge and approaches to zero with $ZnSO_4$ concentration increase, while that of the Al_2O_3 nanoparticles increases a positive charge. Therefore, approaching to zero potential with salt concentration increase in SiO_2 nanoparticles/$ZnSO_4$·$n$$H_2O$ system might be related to the behavior of T_1 as shown in Fig.

10; subtle volume fraction dependences and approaches to the bulk value with $ZnSO_4$ concentration increase. It was assumed that the effects from solid phase in solid/liquid coexisting system were affected by liquid property in itself.

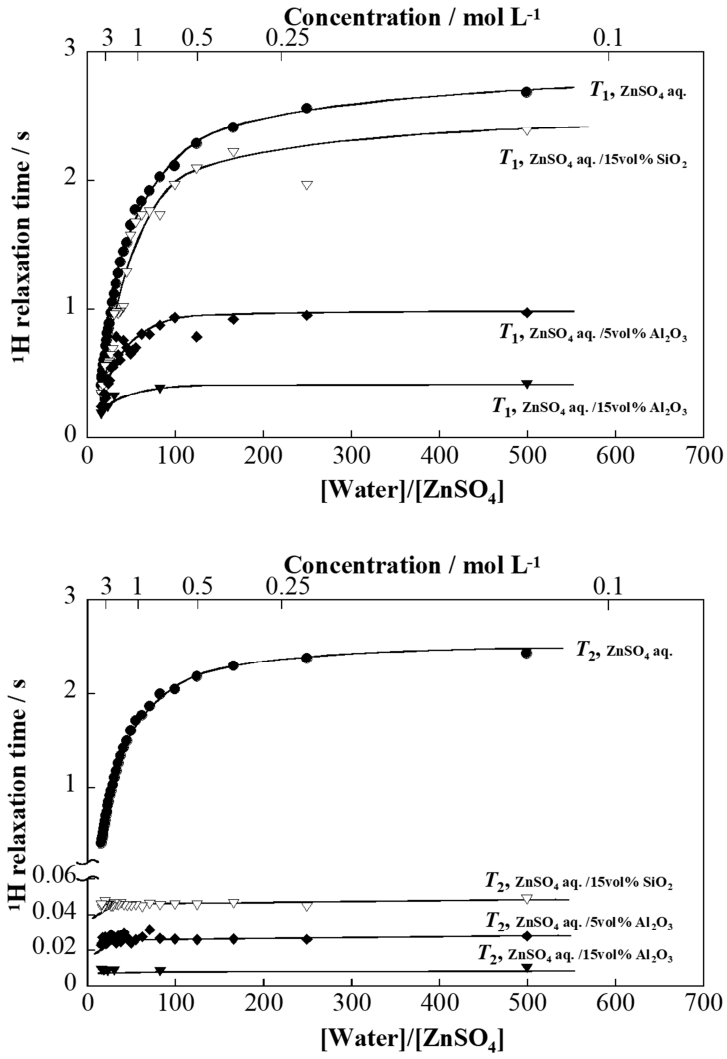

Figure 12. Concentration and numerical ratio dependences of ^1H relaxation time (T_1, T_2) for SiO_2 and Al_2O_3 nanoparticles/$ZnSO_4{\cdot}nH_2O$ system; (a) T_1 and (b) T_2. The hydration number n represents the numerical ratio; [Water]/[$ZnSO_4$] in the figure.

Conclusion

Properties of metal oxide nanoparticles/$ZnSO_4{\cdot}nH_2O$ system were discussed within wide salt concentration range from dilute to concentrated solution. Numerical ratio of water molecules per one salt and apparent average thickness were employed to describe the liquid behavior in the vicinity of solid surface. The H_2O-$ZnSO_4$ system showed phase diagram which have eutectic composition at mole fraction of $ZnSO_4$ was 0.050 from DSC results. The volume increment by water molecules per one salt derived from density measurement represented strong interaction by electrostriction of $ZnSO_4$. Raman spectroscopy in solid/liquid coexisting system suggested that ion paring tendencies were

enhanced in vicinal area of solid surface. From the relationship between ^{1}H relaxation in $ZnSO_4$ aq. and surface potential of metal oxide nanoparticles, water molecules in aqueous solution was affected by not only ionic interaction but also coexisting solid surface, and alumina exhibited strong effect than silica. Different behavior of ^{1}H relaxation in coexisting systems between silica and alumina might be due to the surface potential of each solid particles depending on pH of liquid phase.

References

1. W. Drost-Hansen, *Ind. Eng. Chem.*, **61**(11), 10 (1969).
2. M. Mizuhata, T. Ohashi and A. B. Béléké, *Int. J. Hydrogen Energy*, **37**, 19407 (2012).
3. M. Mizuhata, F. Ito and S. Deki, *J. Power Sources*, **146**, 365 (2005).
4. S. Deki, M. Mizuhata, S. Nakamura, A. Kajinami and Y. Kanaji, *J. Electrochem. Soc.*, **139**, 996 (1992).
5. Y. Yamada, K. Usui, K. Sodeyama, S. Ko, Y. Tateyama and A. Yamada, *Nat. Energy*, **1**, 16129 (2016).
6. L. Suo, O. Borodin, T. Gao, M. Olguin, J. Ho, X. Fan, C. Luo, C. Wang and K. Xu, *Science.*, **350**, 938 (2015).
7. L. Suo, O. Borodin, Y. Wang, X. Rong, W. Sun, X. Fan, S. Xu, M. A. Schroeder, A. V. Cresce, F. Wang, C. Yang, Y. S. Hu, K. Xu and C. Wang, *Adv. Energy. Mater.*, 1701189 (2017)
8. J. Braunstein, *Inorg. Chim. Acta Rev.,* **2**, 19 (1968).
9. J. S. Weston, D. Venkataramani, C. P. Aichele, B. P. Grady, J. Harewell and D. Resasco, *Langmuir*, **30**, 14982 (2014).
10. M. Farahmandjou and N. Golabiyan, *J. Ceram. Process. Res.*, **16**(2), 1 (2015).
11. A. Moiseev, F. Qi, J. Deubener and A. Weber, *Chem. Eng. J.*, **170**, 308 (2011).
12. R. Kanagadurai, R. Durairajan, R. Sankar, G. Sivanesan, S. P. Elangovan and R. Jayavel, *E-J Chem.*, **6**(3), 871 (2009).
13. W. W. Rudolph and C. C. Pye, *Phys. Chem. Chem. Phys.,* **1**, 4583 (1999).
14. W. W. Ewing, N. L. Krey, H. Law and E. Lang, *J. Am. Chem. Soc.,* **49**(8), 1958 (1927).
15. E. Hennings, P. Zürner, H. Schmidt and W. Voigt, *Icarus*, **226**, 268 (2013).
16. M. C. Iliuta, K. Thomsen and P. Rasmussen, *AlChE Journal*, **48**, 11 (2002).
17. J. Pátek and J. Klomfar, *Fluid Phase Equilibria*, **250**, 138 (2006).
18. A. N. Campbell and R. A. Bailey, *Can. J. Chem.*, **36**, 518 (1958).
19. Y. Marcus, *Chem. Rev.*, **111**, 2761 (2011).
20. M. Mizuhata, Y. Sumihiro and S. Deki, *Phys. Chem. Chem. Phys.,* **6**, 1944 (2004).
21. M Zobel, *Acta Cryst.*, **A72**, 621 (2016).
22. W. W. Rudolph, M. H. Brooker and P. Tremaine, *Zeitschrift für Physikalische Chmie.,* **209**, 181 (1999).
23. W. W. Rudolph, M. H. Brooker and P. Tremaine, *J. Solution Chem.*, **28**(5), 621 (2005).
24. W. W. Rudolph and C. C. Pye, *J. Solution Chem.*, **28**(9), 1045 (2005).